Chapter 16

Redox Driven Stable Isotope Fractionation

Jay R. Black,[1,*] Jeffrey A. Crawford,[1] Seth John,[3] and Abby Kavner[1,2]

[1]Institute for Geophysics and Planetary Physics, [2]Earth and Space Sciences, University of California, Los Angeles, 595 Charles E. Young Drive East, Los Angeles, CA 90095
[3]Department of Earth and Ocean Sciences, University of South Carolina, Columbia, SC 29208
[*]jayblack@ucla.edu

Electrochemical reduction/oxidation (redox) reactions have been observed to drive stable isotope fractionation in many metal systems, where the lighter isotopes of a metal are typically partitioned into the reduced chemical species. While physical processes such as diffusive mass transport lead to small isotope fractionations, charge transfer processes can lead to isotope fractionations up to ten times larger and twice that predicted by equilibrium stable isotope theory. Control over physical and chemical variables during electrochemical experiments, such as overpotential and temperature, allow for the isotopic composition of deposited metals to be fine tuned to a specific value.

Introduction

Redox reactions drive many chemical transformations in the environment, and are vital in biological cycles for energy production. Many elements are redox sensitive, with multiple accessible oxidation states stable in a variety of environments. The transition metal elements are of particular interest, as some of the largest stable isotope fractionations seen in these metal systems are associated with redox transformations. Therefore, stable isotope signatures may be used for a wide range of applications, from studying the transport and deposition of metals in the environment for the purposes of monitoring and remediation of contaminants, to reconstructing the chemistry of our planet in the past. In order

In Aquatic Redox Chemistry; Tratnyek, P., et al.;
ACS Symposium Series; American Chemical Society: Washington, DC, 2011.

to do this, an understanding of what drives stable isotope fractionation during a redox reaction is needed.

The history behind the discovery of deuterium is a good starting point, as it was after its discovery by Harold Urey (*1*) that the first electrolytically produced sample of heavy water was reported by Gilbert N. Lewis and Ronald T. MacDonald (*2*) who concentrated 20 liters of normal abundance water down to 0.5 ml of 66% deuterium through electrolysis. The electrochemical separation of stable isotopes subsequently became one of the earliest industrialized forms of stable isotope purification, with pure deuterium being produced using electrolytic cells in cascade reactors (*3–5*). The fractionation factor of industrial electrolytic cells varied as a function of the cell geometry and physical parameters, such as temperature and overpotential used, from $\alpha_{liquid\text{-}vapor}$ = 3 to 13 (*4*, *5*) (where $\alpha = D/H_{liquid}/D/H_{vapor}$). The electrochemical separation of ^{6}Li and ^{7}Li was later developed showing smaller fractionation factors of approximately $\alpha_{aqueous\text{-}metal}$ = 1.020-1.079, where $\alpha = {}^{7}Li/{}^{6}Li_{aqueous}/{}^{7}Li/{}^{6}Li_{metal}$ (*6*, *7*). The accepted theory to explain these fractionations was that they were due to a difference in the equilibrium potential for the reduction of one isotopologue species over another, leading to a 'kinetic isotope effect' far from equilibrium (*5*). Quantum-mechanical tunneling may also play a role in the case of hydrogen fractionations (*8*), altering the reaction coordinate for isotopologue species. Interest in separating lithium isotopes for the nuclear fuel industry has sparked recent interest in using electrochemical methods for the task (*9–13*). Recent experiments by Kavner and co-workers (*14–19*) have developed our understanding of the physical and chemical controls upon isotope fractionation during electrochemical experiments and form the basis for discussion in this chapter.

Figure 1 illustrates the electric double layer at an electrode surface and the physical and chemical processes that may contribute to the fractionation of stable isotopes during an electrochemical reaction. These include equilibria between different chemical species in solution or at the surface of the electrode, diffusion of reactant to the electrode surface, and finally the charge transfer kinetics at the electrode surface. Stable isotope ratios are reported here in a delta notation (Figure 1), with units of permil (‰) expressing the difference in isotopic ratio of a sample to a standard:

$$\delta^{X/Y}M = \left(\frac{{}^{X/Y}M_{sample}}{{}^{X/Y}M_{standard}} - 1 \right) \cdot 1000 \qquad (1)$$

$$\Delta^{X/Y}M_{A\text{-}B} = \delta^{X/Y}M_{A} - \delta^{X/Y}M_{B}$$

where $^{X/Y}M$ is often reported as the ratio of a heavy isotope over a light isotope, (e.g., $^{56/54}Fe$, $^{66/64}Zn$ and $^{7/6}Li$) therefore, positive and negative $\delta^{X/Y}M$ indicate a sample which contains more of the heavy and light isotope of an element relative to a standard, respectively. The capital delta notation reflects the isotopic difference (in permil) between two substances, A and B.

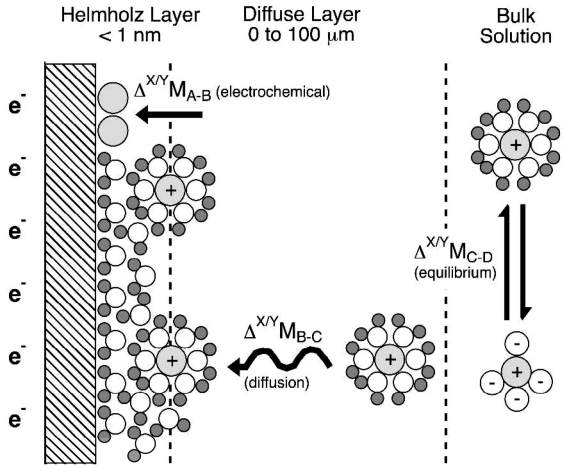

Figure 1. Schematic of the electric double layer adjacent to the surface of an electrode. The processes that may contribute to the overall isotopic signature in the plated (substance A) metal are labeled next to the arrows (19). Substance B = surface adsorbed reactant species; C = diffusing reactant species; D = secondary bulk solution species.

Combining Marcus Theory with Equilibrium Stable Isotope Theory

In a series of papers investigating iron and zinc stable isotope fractionation during electrodeposition Kavner et al. (*14*, *15*) derived an equation which combined equilibrium stable isotope theory (*20–22*) with Marcus's statistical mechanic description of charge transfer processes at an electrode (*23*):

$$\ln \alpha_{metal-aqueous} = \ln\left(\frac{k'}{k}\right) = \ln\left(\frac{v'}{v}\right) + \left(\frac{\Delta G^{*} - \Delta G^{*'}}{k_B T}\right)$$
$$= \frac{1}{2}\ln\left(\frac{m}{m'}\right) + \left(\frac{\ln \alpha_{eq}}{2} - \frac{k_B T\left(\ln \alpha_{eq}\right)^2 + 2k_B T \ln\left(Q_P / Q_R\right)\ln \alpha_{eq} + 2\eta z e \ln \alpha_{eq}}{4\lambda}\right) \quad (2)$$

where isotopic fractionation ($\ln \alpha_{metal\text{-}aqueous}$) depends on the charge transfer rate (k) for metal deposition ($^{light}M^{z+}_{(aq)} + ze^- = {}^{light}M_{(s)}$), collision frequency ($v$), activation free energy (ΔG^*), Boltzmann's constant (k_B), temperature (T), mass in motion (m), equilibrium fractionation factor (α_{eq}), partition function ratio of abundant isotopologues of product and reactant (Q_P/Q_R), number of electrons (z), charge of an electron (e), and Marcus reorganization energy (λ) (*9*). The primed symbols are for the corresponding heavy isotopologue charge transfer reaction ($^{heavy}M^{z+}_{(aq)} + ze^- = {}^{heavy}M_{(s)}$).

Equation 2 makes a number of testable predictions about how stable isotopes are fractionated during a charge transfer reaction:

- Fractionation is linearly dependent upon applied voltage (overpotential = $\eta = E\text{-}E^0$) or, in other words, the driving force or extent of disequilibrium.
- The magnitude and slope of the fractionation scales with the equilibrium fractionation factor between product and reactant divided by the Marcus reorganization energy.
- Fractionation decreases with increasing temperature, primarily controlled by the change in magnitude of the equilibrium fractionation factor, which scales proportionally with $1/T^2$ under most circumstances (*24*), but not in all cases (*25*).

To test these predictions, electrochemical experiments were conducted where a number of the variables of interest could be controlled including the solution chemistry, temperature, and applied overpotential. Other properties such as the effect of mass transport of reactant to the electrode surface were tested by the use of planar electrodes in unstirred solutions compared with controlled hydrodynamic conditions using a rotating disc electrode. Here we present and summarize the results of previous electrochemical experiments (see following section) and the results of new experiments where copper is electroplated on rotating disc electrodes as a function of temperature, overpotential and electrode rotation rate.

Prior Experimental Results

Results from previously published electrodeposition experiments where metal was deposited on planar electrodes are shown in Figure 2, which plots results for $\Delta^{66/64}Zn_{metal\text{-}aqueous}$ and $\Delta^{56/54}Fe_{metal\text{-}aqueous}$ on the left hand axis and $\Delta^{7/6}Li_{metal\text{-}solution}$ on the right hand axis versus the applied overpotential. The following observations and interpretations can be made:

- In all cases the lighter isotope is preferentially partitioned into the deposited metal, with much larger fractionation factors seen for lithium compared to iron and zinc.
- The observed electrochemical fractionations for iron and zinc are much larger than calculated equilibrium fractionation factors ($\Delta^{56/54}Fe_{metal\text{-}aqueous}$ = -0.9 ‰ (*26*) and $\Delta^{66/64}Zn_{metal\text{-}aqueous}$ = -2.5 ‰ (*27*) at 25°C), especially at lower deposition rates near zero overpotential (Fig. 2). For lithium, fractionation approaches its equilibrium value ($\Delta^{7/6}Li_{metal\text{-}solvated}$ = -29.6 ‰ at room temperature (*28*)) near zero overpotential where fractionation should be controlled by equilibrium processes (Fig. 2). Equilibrium stable isotope theory predicts that fractionation should scale roughly with the difference in mass over the product of the mass of the two isotopes ($\Delta m/m^2$, (*24*)). Therefore it makes sense that the fractionation in lithium deposits is larger on an absolute scale than the Fe and Zn fractionations. However, when the results shown in Figure 2 are normalized to this ratio ($\Delta m/m^2$), the lithium fractionations, which do not exceed the predicted equilibrium

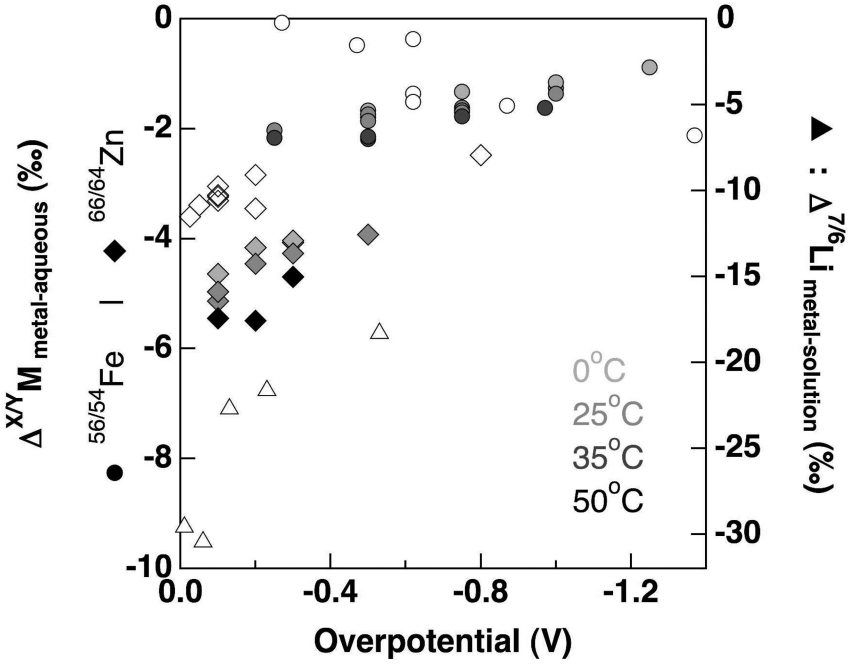

Figure 2. Stable isotope composition of various metals electrodeposited on planar electrodes including Zn (diamonds) (15, 19), Fe (circles) (14, 19) and Li (triangles) (17). Hollow symbols indicate experiments that were not temperature controlled. Filled symbols are temperature controlled experiments.

value (*28*), show smaller mass-relative electrochemical effects than do zinc and iron, which do exceed their equilibrium values.

- When examining the iron and zinc results side by side (Fig. 2) larger fractionations are seen in zinc metal deposits. This result is partly explained by the solvation structure of the metals in solution, as calculated equilibrium fractionation factors for the hexaquo-iron and -zinc complexes (predominant forms of aqueous iron and zinc) relative to metal are $\Delta^{56/54}Fe_{metal\text{-}aqueous}$ = -0.9 ‰ (*26*) and $\Delta^{66/64}Zn_{metal\text{-}aqueous}$ = -2.5 ‰ (*27*) at 25°C. Other discrepancies between experiments arise from different experimental designs.
- Fractionations were different in stagnant solutions (hollow markers, Fig. 2) compared to stirred solutions (solid markers, Fig. 2). Comparing trends in the zinc data (diamonds, Fig. 2) between the hollow (*15*) and solid marker samples (*19*), where the same solution chemistry was used, shows an almost 1.5 ‰ difference in the isotopic composition of samples. Temperature cannot account for this large discrepancy between the experiments and so this indicates that the stirring of solutions may have a large effect on the observed fractionation.
- Temperature trends in the solid marker data sets (Fig. 2) are unusual, with fractionation increasing with increasing temperature in both the iron and

zinc experiments, while equilibrium stable isotope theory predicts that fractionation should decrease at higher temperatures as $1/T^2$ (*24*).

- The trend in fractionation versus overpotential for iron samples (circles, Fig. 2) changes depending on experimental conditions, with fractionation increasing at increasing applied overpotential in stagnant experiments (*14*) and decreasing with increasing applied overpotential in stirred experiments (*19*). The solution chemistry may partly explain the differences in the case of iron, as the pH of solutions in stagnant experiments was lower (pH < 1) compared to stirred experiments (pH ~ 2.5) and this affected the iron deposition efficiency relative to $H_{2(g)}$ production at the cathode.

Experimental Methods

Sample Solution Preparation

A 1 L stock solution of 0.7 M copper sulfate was prepared from a $CuSO_4.5H_2O$ salt (pH = 3.05). Fresh 50 mL aliquots were taken from this stock for every second to fourth experiment (stock solution compositions before and after samples runs were monitored to ensure there was no Rayleigh-type evolution of the reservoirs).

Electrodeposition Experiments

Electrochemical parameters were controlled by an Autolab potentiostat (PGSTAT30) using a platinum rotating disc working electrode (3 mm diameter), a platinum counter electrode, and a Ag/AgCl double junction reference electrode (filled with 3 m KCl). The electrodes were immersed in ~50 mL of degassed sample solution and the temperature of this solution was controlled by an external water bath. The equilibrium potential (E^0) of sample solutions in the electrochemical cell were experimentally determined using cyclic voltammetry with variable sweep rates. A series of electrodeposition experiments were performed as a function of: applied overpotential ($E-E^0$); time (one Coulomb of charge being delivered in all cases, regardless of the rate of reduction which varied with overpotential); temperature; and electrode rotation rate, summarized in Table 1.

Samples of electroplated copper were dissolved in warm 2% (w/v) HNO_3 in Teflon cups. The samples were then evaporated to dryness and diluted with 4 mL of 2% HNO_3. Before isotopic analysis (see below) the samples were diluted to a final concentration of 20 ppm copper. Dilutions were measured for Cu concentrations to provide an estimate of the total amount of metal electroplated. A comparison between this value and the total amount of charge passed provides a lower bound estimate of the efficiency of the plating reaction and in all cases was ~108 % ± 7% (2σ); therefore efficiencies are taken as 100% in all cases.

Table 1. Summary of electrochemical experiments and MC-ICP-MS results

Sample	*Temp. (°C)*	*η (V)[a]*	*Stir Rate (rpm)*	*Average Current (mA)*	*$\Delta^{65/63}$Cu (‰) ± 2σ[b]*
Cu01	0	-0.2	5000	-0.98	-2.17 ± 0.02
Cu02	0	-0.2	10000	-0.91	-2.31 ± 0.02
Cu03	0	-0.3	5000	-1.92	-2.27 ± 0.02
Cu04	0	-0.3	10000	-1.90	-2.22 ± 0.02
Cu05	0	-0.5	2500	-4.25	-2.02 ± 0.02
Cu06	0	-0.5	5000	-4.24	-2.11 ± 0.02
Cu07	0	-0.5	7500	-4.31	-2.10 ± 0.02
Cu08	0	-0.5	10000	-4.36	-2.13 ± 0.02
Cu09	25	-0.1	5000	-1.57	-2.83 ± 0.02
Cu10	25	-0.1	10000	-1.64	-2.74 ± 0.02
Cu11	25	-0.15	5000	-2.75	-2.62 ± 0.02
Cu12	25	-0.15	10000	-2.39	-2.33 ± 0.02
Cu13	25	-0.2	5000	-4.03	-2.28 ± 0.02
Cu14	25	-0.2	10000	-3.05	-2.09 ± 0.02
Cu15	25	-0.3	5000	-5.32	-1.84 ± 0.02
Cu16	25	-0.3	10000	-1.69	-2.48 ± 0.02
Cu17	25	-0.5	2500	-9.25	-1.70 ± 0.02
Cu18	25	-0.5	5000	-9.34	-1.76 ± 0.02
Cu19	25	-0.5	7500	-9.61	-1.84 ± 0.02
Cu20	25	-0.5	10000	-9.51	-1.84 ± 0.02
Cu21	25	-1.0	2500	-21.23	-1.34 ± 0.02
Cu22	25	-1.0	5000	-20.79	-1.54 ± 0.02
Cu23	25	-1.0	7500	-20.79	-1.61 ± 0.02
Cu24	25	-1.0	10000	-20.79	-1.68 ± 0.02
Cu25	50	-0.2	5000	-6.49	-2.40 ± 0.02
Cu26	50	-0.2	10000	-6.57	-2.41 ± 0.02
Cu27	50	-0.3	5000	-10.30	-2.45 ± 0.02
Cu28	50	-0.3	10000	-9.99	-2.29 ± 0.02
Cu29	50	-0.5	2500	-16.92	-1.90 ± 0.02
Cu30	50	-0.5	5000	-18.15	-2.22 ± 0.02

Continued on next page.

Table 1. (Continued). Summary of electrochemical experiments and MC-ICP-MS results

Sample	*Temp. (°C)*	*η (V)*[a]	*Stir Rate (rpm)*	*Average Current (mA)*	$\Delta^{65/63}$*Cu (‰) ± 2σ*[b]
Cu31	50	-0.5	7500	-17.21	-2.10 ± 0.02
Cu32	50	-0.5	10000	-17.83	-2.33 ± 0.02

[a] Overpotential, η, (E – E^0) relative to measured E^0 from CV spectra; [b] The isotopic composition of all samples were measured in triplicate with the exception of Cu27 which was only measured in duplicate.

Isotope Analysis

Isotopic analyses were performed using a Thermo-Finnigan Neptune Multi-collector Inductively Coupled Plasma Mass Spectrometer. Samples were introduced via a cyclonic spray chamber. Samples and standards were diluted to a Cu concentration of 20 ppm and spiked with 20 ppm of an in-house Zn standard. Samples were run alternately with a NIST SRM 682 Zn standard, also spiked with Cu, which has previously been compared to JMC 3–0749L Zn (*29*). Signal intensity on ^{60}Ni, ^{63}Cu, ^{64}Zn, ^{65}Cu, ^{66}Zn and ^{68}Zn were monitored on cups L3, L2, L1, C, H1, and H2, respectively. Samples and standards were run alternately for three minutes each, with 3 minutes rinsing in between. Monitoring of the measured Zn isotope ratio in samples showed that there was no significant mass bias due to matrix effects in copper samples compared to standards. Samples were therefore corrected for instrumental mass bias using only sample-standard bracketing. Table 1 summarizes the isotopic composition of samples relative to stock solutions. In all experiments the isotopic composition of the stock solution was unchanged within experimental error before and after an electroplating experiment. This establishes a constant isotope reservoir, with no effects from Rayleigh-type compositional evolution.

Results and Discussion

To better understand the trends described in the previous experiments (Figure 2), the experiments presented here were designed with control over several different parameters including the rate at which solution was advected over the electrode (controlled by using a rotating disc electrode), solution chemistry, the applied overpotential and temperature. Figure 3 presents the isotopic composition of copper metal samples as a function of the temperature (Fig. 3A) and electrode rotation rate (Fig. 3B). The calculated equilibrium fractionation between a copper hexaaquo complex and metallic copper (RPFR estimated from frequency calculations for the optimized aqueous complex and a literature report of the vibrational density of states for metallic copper (*30*)) is also plotted (dashed line, Fig. 3). The following sections discuss the trends observed in terms of the physical and chemical variables examined in the experiments.

Effect of Temperature

Figure 3A plots the stable isotope composition of copper metal samples from this study as a function of temperature. There is a decrease in the sample fractionation with increasing temperature from 0 to 25°C of ~0.5 ‰, as predicted by the plotted equilibrium fractionation (dashed line, Fig. 3), and the predictions of Equation 2. However, an increase in fractionation is observed at 50°C and may indicate a change in the electrodepostion mechanism or surface chemistry at the electrode.

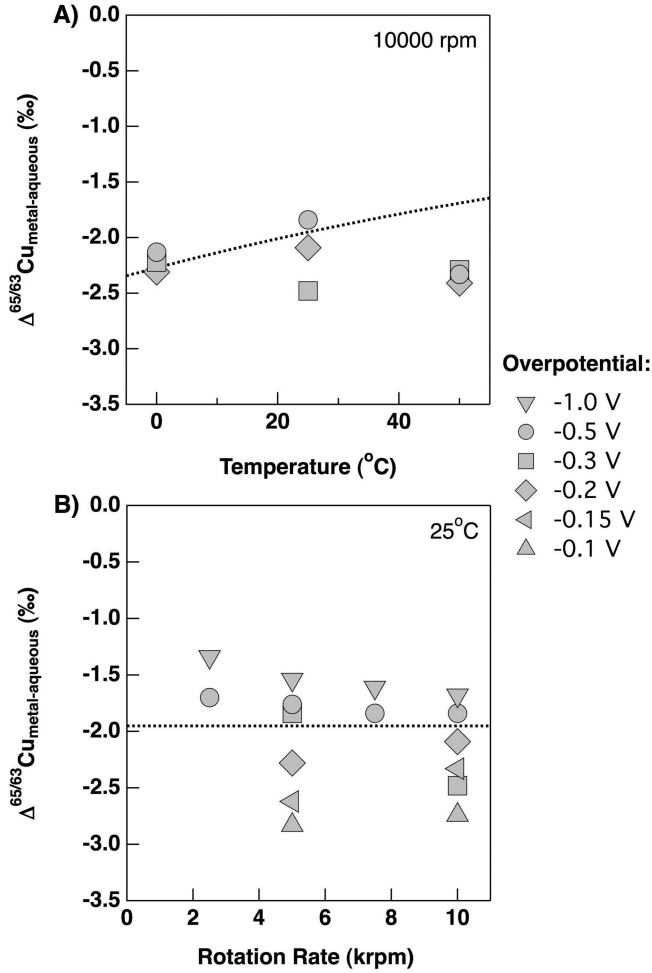

*Figure 3. Stable isotope composition of electrodeposited copper as a function of **A)** temperature; **B)** RDE rotation rate. Dashed line = calculated equilibrium.*

Effect of Mass Transport

Figure 3B plots the stable isotope composition of copper metal samples from this study as a function of the electrode rotation rate at 25°C. At higher overpotentials the same trend is observed of increasing fractionation with increasing rotation rate, and the same trends were observed at higher and lower temperatures and in another study of iron (*18*). Calculation of the magnitude of fractionation due to diffusion across the mass-transport boundary layer (diffuse layer, Fig. 1) at the electrode surface indicate that diffusive limitations would lead to much smaller fractionations for iron and zinc (e.g. $\Delta^{66/64}Zn_{diffusion}$ = -0.27 ‰ (*19*, *31*, *32*)), and copper with a similar solution chemistry and diffusion coefficient is likely to exhibit a similar small diffusive fractionation. This explains some of the trends observed with temperature and rotation rate. Under diffusive control the fractionation in metal samples will be attenuated by the smaller fractionation associated with diffusion to the reactive interface. As temperature increases and rotation rate increases fractionation will also increase because diffusion occurs more quickly at higher temperatures and the width of the diffusive sublayer decreases at higher rotation rates, so that diffusion no longer attenuates the large electrochemical isotope effects as much. This effect can be quantified by plotting isotope fractionation against the ratio of observed current at the cathode versus a calculated diffusion limiting current (Figure 4) given by the Levich equation (*32*). Figure 4 shows that the data falls along a trend of increasing fractionation with decreasing current ratio (i.e. as reaction kinetics dominate over diffusion limitations fractionation increases) and resolves the temperature and rotation rate effects observed.

Effect of Electrochemical Variables

Amount Plated

In the copper deposition experiments presented here one Coulomb of metal was plated in all cases. However, it was shown in previous studies (*9*, *10*, *14*) that varying the amount of charge delivered from 5 (0.5 minute) to 50 (5 minutes) Coulombs with all other variables fixed, led to no change in the observed fractionation in metal within the experimental error.

Overpotential

Figure 3 plots data collected at different applied overpotentials as different symbols, showing a general trend towards smaller fractionations in the copper metal with increasing overpotential. The same trends were seen in previous experiments (Fig. 2 (*15*, *17*, *19*)) with the exception of one study (hollow circular symbols, Fig. 2 (*14*)). Figure 3 clearly illustrates that at low overpotentials the fractionation in samples is larger than predicted by equilibrium stable isotope theory (dashed line, Fig. 3), and is therefore suggestive of a kinetic isotope effect. However, with increasing overpotential (i.e., increasing disequilibrium)

the fractionation in samples decreases below this equilibrium fractionation line. As discussed in the introduction, Equation 2 predicts that fractionation scales linearly with the applied overpotential, however, closer inspection of the trends in the data do not show a perfectly linear dependence. This may be partly explained by concurrent isotope effects, such as diffusive limitations of reactant to the electrode interface where reaction occurs. Diffusive limitations may also explain the smaller fractionations observed further from equilibrium at higher applied overpotentials.

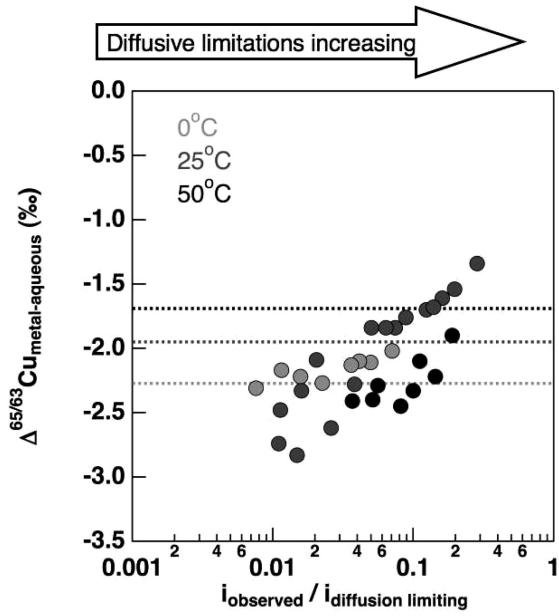

Figure 4. Stable isotope composition of electrodeposited copper as a function of the current ratio of observed to calculated diffusion limiting current. Dashed lines represent calculated equilibrium fractionation at different temperatures.

Conclusions

Large fractionation of metal stable isotopes are observed during redox reactions. These fractionations are not controlled by a single process, but instead result from the interaction between several different processes, each of which can fractionate isotopes on their own and/or moderate the fractionations caused by other processes. Under experimental conditions, three chemical and physical processes dominate these stable isotope fractionations:

1) Equilibrium isotope effects between different chemical species, leading to smaller fractionations at higher temperatures, scaling as $1/T^2$ under most circumstances.

In Aquatic Redox Chemistry; Tratnyek, P., et al.;
ACS Symposium Series; American Chemical Society: Washington, DC, 2011.

2) Electrochemical kinetic isotope effects, where differences in the activation energy for charge transfer lead to large isotope effects.
3) Diffusive isotope effects, which are small in comparison to these other effects and which increase at higher temperatures.

The relative difference in magnitude of these effects can be used to predict and produce isotopic products of metals of specifically tuned composition by controlling the mass transport, temperature and reaction kinetics of a given system. Understanding the interaction between these processes also provides a framework for interpreting isotopic signals in nature, where the magnitude of fractionation may be used to distinguish between kinetic and equilibrium effects, or to determine under what natural conditions reactions become diffusion limited. Many of the chapters in this volume discuss various pathways involving redox transformations of iron. Chapters 8 (*33*) and 9 (*34*) discuss reactions of iron with reactive oxygen species in aquatic systems, chapter 14 (*35*) discusses how complexation of iron to organic ligands mediates redox reactions between the Fe(II)-Fe(III) couple, chapters 13 (*36*) and 15 (*37*) discuss sorption of iron to FeS adlayers and ferric oxide minerals followed by redox activity, chapter 17 (*38*) looks at how the structural properties of clays change with the oxidation and reduction of iron within the structure, and chapter 18 (*39*) looks at the reactivity of zero valent iron in the environment and its importance in reactive-transport models. All of these processes may induce their own unique isotopic signature in the separate redox phases of iron which potentially could be used to study these reaction pathways. Many other redox active metals have their own suite of stable isotopes whose ratios will be affected by their redox cycle.

Acknowledgments

We thank Professor Jess Adkins for access to facilities at Caltech. This work was funded by NASA Exobiology NNG05GQ92G (A.K.) and the U.S. Department of Energy: Division of Chemical Sciences, Geosciences, & Biosciences DE-FG02-10ER16136 (A.K.).

References

1. Urey, H. C.; Brickwedde, F. G.; Murphy, G. M. The hydrogen isotope of mass 2 and its concentration. *Phys. Rev.* **1932**, *40*, 1–15.
2. Lewis, G. N.; Macdonald, R. T. Concentration of H2 isotope. *J. Chem. Phys.* **1933**, *1* (6), 341–344.
3. Rae, H. K. Selecting Heavy Water Processes. In *Separation of Hydrogen Isotopes*; Rae, H. K., Ed.; Americal Chemical Society: Washington, DC, 1978; Vol. 68, pp 1−26.
4. Villani, S. *Separation of Isotopes*; American Nuclear Society: Hinsdale, IL, 1974; p 499.

5. Ishida, T.; Fujii, Y. Enrichment of isotopes. In *Isotope Effects in Chemistry and Biology*; Kohen, A., Limbach, H.-H., Eds.; CRC Press, Taylor & Francis Group: Boca Raton, FL, 2006; pp 41−87.
6. Taylor, T. I.; Urey, H. C. The electrolytic and chemical-exchange methods for the separation of the lithium isotopes. *J. Chem. Phys.* **1937**, *5*, 597–8.
7. Johnston, H. L.; Hutchison, C. A. Efficiency of the electrolytic separation of lithium isotopes. *J. Chem. Phys.* **1940**, *8*, 869–77.
8. Weston, R. E., Jr. Isotope Effects and Quantum-Mechanical Tunneling. In *Isotopes and Chemical Principles*; Rock, P. A., Ed.; American Chemical Society: Washington, DC, 1975; pp 44−63.
9. Fujie, M.; Fujii, Y.; Nomura, M.; Okamoto, M. Isotope effects in electrolytic formation of lithium amalgam. *J. Nucl. Sci. Technol.* **1986**, *23* (4), 330–7.
10. Mouri, M.; Yanase, S.; Oi, T. Observation of Lithium Isotope Effect Accompanying Electrochemical Insertion of Lithium into Zinc. *J. Nucl. Sci. Technol.* **2008**, *45* (5), 384–389.
11. Yanase, S.; Hayama, W.; Oi, T. Lithium Isotope Effect Accompanying Electrochemical Intercalation of Lithium into Graphite. *Z. Naturforsch.* **2003**, *58a*, 306–312.
12. Yanase, S.; Oi, T.; Hashikawa, S. Observation of Lithium Isotope Effect Accompanying Electrochemical Insertion of Lithium into Tin. *J. Nucl. Sci. Technol.* **2000**, *37* (10), 919–923.
13. Zenzai, K.; Yanase, S.; Zhang, Y.-H.; Oi, T. Lithium isotope effect accompanying electrochemical insertion of lithium into gallium. *Prog. Nucl. Energy* **2008**, *50* (2−6), 494–498.
14. Kavner, A.; Bonet, F.; Shahar, A.; Simon, J.; Young, E. The isotopic effects of electron transfer: An explanation for Fe isotope fractionation in nature. *Geochim. Cosmochim. Acta* **2005**, *69* (12), 2971–2979.
15. Kavner, A.; John, S. G.; Sass, S.; Boyle, E. A. Redox-driven stable isotope fractionation in transition metals: Application to Zn electroplating. *Geochim. Cosmochim. Acta* **2008**, *72* (7), 1731–1741.
16. Kavner, A.; Shahar, A.; Black, J. R.; Young, E. Iron Isotopes at an Electrode: Diffusion-Limited Fractionation. *Chem. Geol.* **2009**, *267* (3−4), 131–138.
17. Black, J. R.; Umeda, G.; Dunn, B.; McDonough, W. F.; Kavner, A. The Electrochemical Isotope Effect and Lithium Isotope Separation. *J. Am. Chem. Soc.* **2009**, *131*, 9904–9905.
18. Black, J. R.; Young, E.; Kavner, A. Electrochemically controlled iron isotope fractionation. *Geochim. Cosmochim. Acta* **2010**, *74*, 809–817.
19. Black, J. R.; John, S.; Young, E. D.; Kavner, A. Effect of Temperature and Mass-Transport on Transition Metal Isotope Fractionation During Electroplating. *Geochim. Cosmochim. Acta* **2010**, *74*, 5187–5201.
20. Bigeleisen, J.; Mayer, M. G. Calculation of equilibrium constants for isotopic exchange reactions. *J. Chem. Phys.* **1947**, *15*, 261–7.
21. Urey, H. C. Thermodynamic properties of isotopic substances. *J. Chem. Soc.* **1947**, 562–81.
22. Bigeleisen, J. Nuclear Size and Shape Effects in Chemical Reactions. Isotope Chemistry of the Heavy Elements. *J. Am. Chem. Soc.* **1996**, *118* (15), 3676–80.

23. Marcus, R. A. Electron-transfer reactions in chemistry: theory and experiment (Nobel lecture). *Angew. Chem.* **1993**, *105* (8), 1161–72.
24. Schauble, E. A. Applying stable isotope fractionation theory to new systems. In *Geochemistry of Non-traditional Stable Isotopes*; Johnson, C. M., Beard, B. L., Albarede, F., Eds.; Mineralogical Society of America: Washington, DC, 2004; Vol. 55, pp 65−111.
25. Bigeleisen, J. Temperature dependence of the isotope chemistry of the heavy elements. *Proc. Natl. Acad. Sci. U.S.A.* **1996**, *93* (18), 9393–9396.
26. Schauble, E. A.; Rossman, G. R.; Taylor, H. P. Theoretical estimates of equilibrium Fe-isotope fractionations from vibrational spectroscopy. *Geochim. Cosmochim. Acta* **2001**, *65* (15), 2487–2497.
27. Black, J. R.; Kavner, A.; Schauble, E. A. Calculation of Equilibrium Stable Isotope Partition Function Ratios for Aqueous Zinc Complexes and Metallic Zinc. *Geochim. Cosmochim. Acta* **2011**, *75*, 769–783.
28. Singh, G.; Hall, J. C.; Rock, P. A. Thermodynamics of lithium isotope exchange reactions. II. Electrochemical investigations in diglyme and propylene carbonate. *J. Chem. Phys.* **1972**, *56* (5), 1855–62.
29. John, S. G.; Park, J. G.; Zhang, Z.; Boyle, E. A. The isotopic composition of some common forms of anthropogenic zinc. *Chem. Geol.* **2007**, *245* (1−2), 61–69.
30. Durukanoglu, S.; Kara, A.; Rahman, T. S. Vibrational modes and relative stability of stepped surfaces of copper. *NATO ASI Ser., Ser. B* **1997**, *360*, 599–605.
31. Rodushkin, I.; Stenberg, A.; Andren, H.; Malinovsky, D.; Baxter, D. C. Isotopic Fractionation during Diffusion of Transition Metal Ions in Solution. *Anal. Chem.* **2004**, *76* (7), 2148–2151.
32. Bard, A. J.; Faulkner, L. R. *Electrochemical Methods: fundamentals and applications*, 2nd ed.; John Wiley & Sons, Inc.: USA, 2001.
33. Garg, S.; Rose, A. L.; Waite, T. D. Pathways Contributing to the Formation and Decay of Ferrous Iron in Sunlit Natural Waters. In *Aquatic Redox Chemistry*; Tratnyek, P. G., Grundl, T. J., Haderlein, S. B., Eds.; ACS Symposium Series; American Chemical Society: Washington, DC, 2011; Vol. 1071, Chapter 8, pp 153−176.
34. Remucal, C. K.; Sedlak, D. L. The Role of Iron Coordination in the Production of Reactive Oxidants from Ferrous Iron Oxidation by Oxygen and Hydrogen Peroxide. In *Aquatic Redox Chemistry*; Tratnyek, P. G., Grundl, T. J., Haderlein, S. B., Eds.; ACS Symposium Series; American Chemical Society: Washington, DC, 2011; Vol. 1071, Chapter 9, pp 177−197.
35. Strathman, T. J. Redox Reactivity of Organically Complexed Iron(II) Species with Aquatic Contaminant. In *Aquatic Redox Chemistry*; Tratnyek, P. G., Grundl, T. J., Haderlein, S. B., Eds.; ACS Symposium Series; American Chemical Society: Washington, DC, 2011; Vol. 1071, Chapter 14, pp 283−313.
36. Helz, G. R.; Ciglenecki, I.; Krznaric, D.; Bura-Nakic, E. Voltammetry of Sulfide Nanoparticles and the FeS(aq) Problem. In *Aquatic Redox Chemistry*; Tratnyek, P. G., Grundl, T. J., Haderlein, S. B., Eds.; ACS Symposium Series;

American Chemical Society: Washington, DC, 2011; Vol. 1071, Chapter 13, pp 265−282.
37. Gorski, C. A.; Scherer, M. M. Fe^{2+} Sorption at the Fe Oxide-Water Interface: A Revised Conceptual Framework. In *Aquatic Redox Chemistry*; Tratnyek, P. G., Grundl, T. J., Haderlein, S. B., Eds.; ACS Symposium Series; American Chemical Society: Washington, DC, 2011; Vol. 1071, Chapter 15, pp 315−343.
38. Neumann, A.; Sander, M.; Hofstetter, T. B. Redox properties of structural Fe in smectite clay minerals. In *Aquatic Redox Chemistry*; Tratnyek, P. G., Grundl, T. J., Haderlein, S. B., Eds.; ACS Symposium Series; American Chemical Society: Washington, DC, 2011; Vol. 1071, Chapter 17, pp 361−379.
39. Tratnyek, P. G.; Salter-Blanc, A. J.; Nurmi, J. T.; Baer, D. R.; Amonette, J. E.; Liu, J.; Dohnalkova, A. Reactivity of zerovalent metals in aquatic media: Effects of organic surface coatings. In *Aquatic Redox Chemistry*; Tratnyek, P. G., Grundl, T. J., Haderlein, S. B., Eds.; ACS Symposium Series; American Chemical Society: Washington, DC, 2011; Vol. 1071, Chapter 18, pp 381−406.